

Supplement of Atmos. Meas. Tech., 13, 3787–3798, 2020
<https://doi.org/10.5194/amt-13-3787-2020-supplement>
© Author(s) 2020. This work is distributed under
the Creative Commons Attribution 4.0 License.



Supplement of

Counting on chemistry: laboratory evaluation of seed-material-dependent detection efficiencies of ultrafine condensation particle counters

Peter Josef Wlasits et al.

Correspondence to: Paul Martin Winkler (paul.winkler@univie.ac.at)

The copyright of individual parts of the supplement might differ from the CC BY 4.0 License.

Table S1. Selected Physical Properties of the Working Fluids: The table shows the diffusion coefficients, dipole moments and dielectric constants of the used working fluids.

Working Fluid	Diffusion Coefficient [cm^2/s]	Dipole Moment [$\mu \cdot 10^{30}/\text{Cm}$]	Dielectric Constant []
N-Butanol	0.0920 ¹	5.8 ³	17.51 ³
Diethylene Glycol	0.0849 ¹	7.0 ³	31.69 (20 °C) ³
Water	0.380 ²	6.2 ³	78.36 ³

¹ Iida et al. (2009), *Aerosol Sci. Tech.*,43:1

² National Center for Biotechnology Information. PubChem Database. Water, CID=962, accessed on 18.11.2019

³ C. Reichardt and T. Welton (2010), *Solvents and Solvent Effects in Organic Chemistry*, Wiley VCH

Table S2. Temperatures of the Tube Furnace: The table displays the minimum and maximum temperatures of the tube furnace that have been set in order to generate particles with mobility diameters between 1 and 25 nm.

Seed Material	T_{min} [K]	T_{max} [K]
NaCl	793.15	873.15
Ag	1073.15	1193.15
(NH ₄) ₂ SO ₄	463.15	513.15

Table S3. The table summarizes the geometrical parameters of the used nano DMA.

Inner Diameter R_i	0.0175 m
Outer Diameter R_o	0.0241 m
Length L	0.0150 m

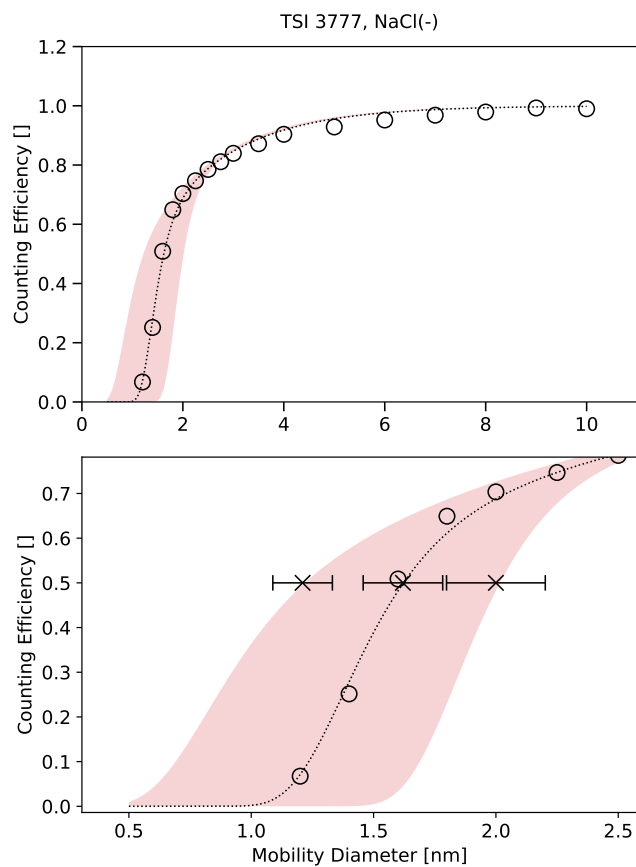


Figure S1. The Figure shows the envelope of the detection efficiency of the TSI 3777 with NaCl seeds. The black circles and the black line depict the curve presented in the manuscript. The black crosses mark the 50% cut-off diameters as well as their deviation due to diffusional broadening of the transfer function of the DMA (based on Reischl et al. (1997)).

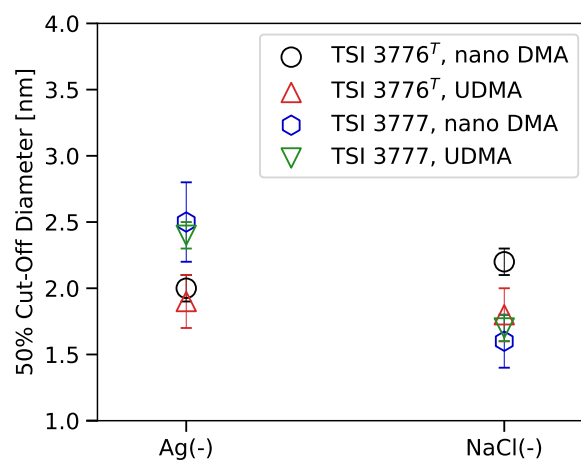


Figure S2. Comparison between nano DMA and UDMA Measurements: The Figure shows the 50 % cut-off diameters for negatively charged Ag and NaCl seeds measured with the TSI 3776^T and the TSI 3777. The spherical markers refer to data obtained by using the a nano DMA as described in Section 2. The triangles represent data measured with an UDMA setup (s. Brilke et al., 2020).

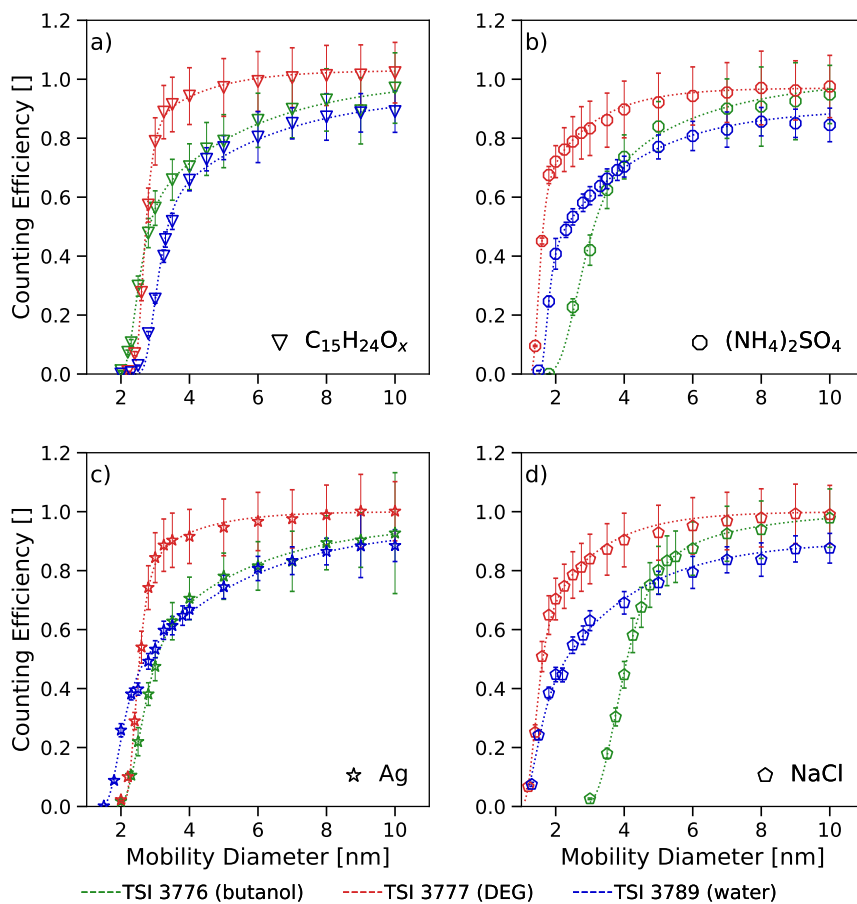


Figure S3. Detection Efficiencies and Seed Particle Material: The Figure shows the detection efficiencies based on different working fluids as a function of the electrical mobility equivalent diameter. Different colors correspond to different particle counters and every plot is related to a different seed particle material: BCY (Panel a), ammonium sulfate (Panel b), silver (Panel c) and sodium chloride (Panel d).

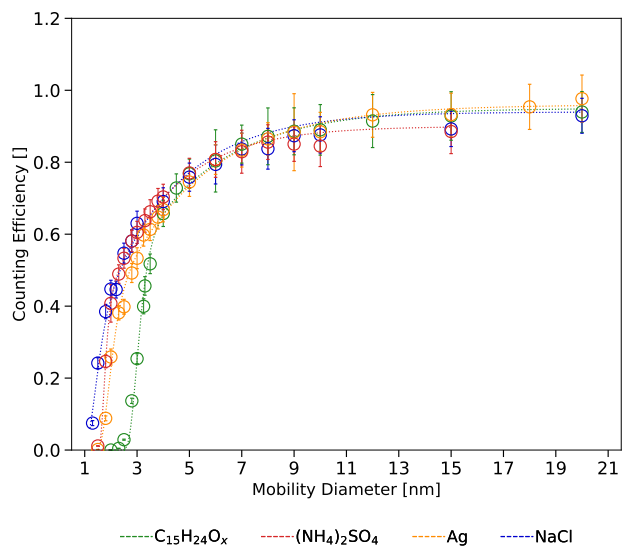


Figure S4. Detection Efficiencies of the TSI 3789: The Figure shows the detection efficiencies for different seed particle materials as a function of the electrical mobility equivalent diameter. Different colors correspond to different seed particles.

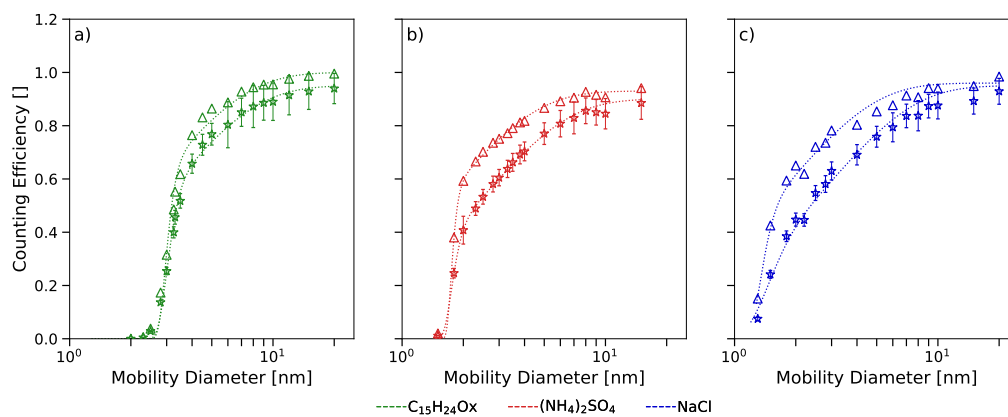


Figure S5. Corrected Detection Efficiencies: The Figure shows detection efficiency data of the TSI 3789 for $BCYO_x$ seeds (Panel a), $(NH_4)_2SO_4$ seeds (Panel b) and NaCl seeds (Panel c), that have been corrected for diffusional losses.

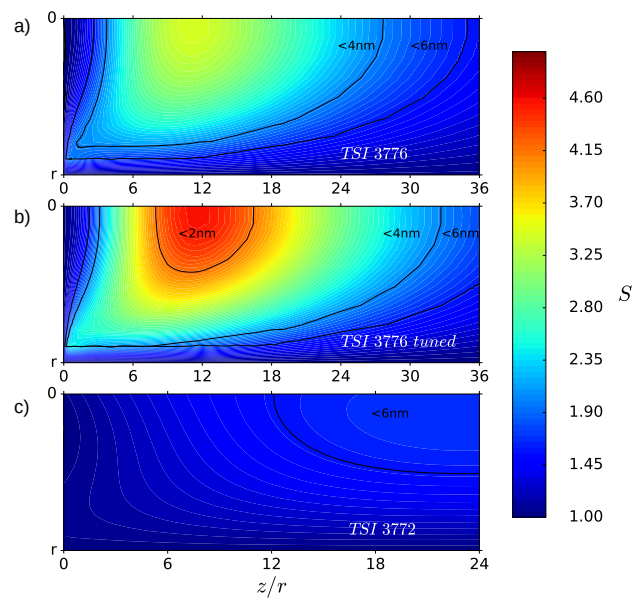


Figure S6. Supersaturation Profiles of Three CPCs: The Figure shows the supersaturation profiles of the TSI 3776 (Panel a), the tuned TSI 3776 (Panel b) and the TSI 3772 (Panel c). The abscissa corresponds to the axial distance on the centerline of the condenser and the ordinate depicts the radial distance. The colors correspond to different saturation ratios.

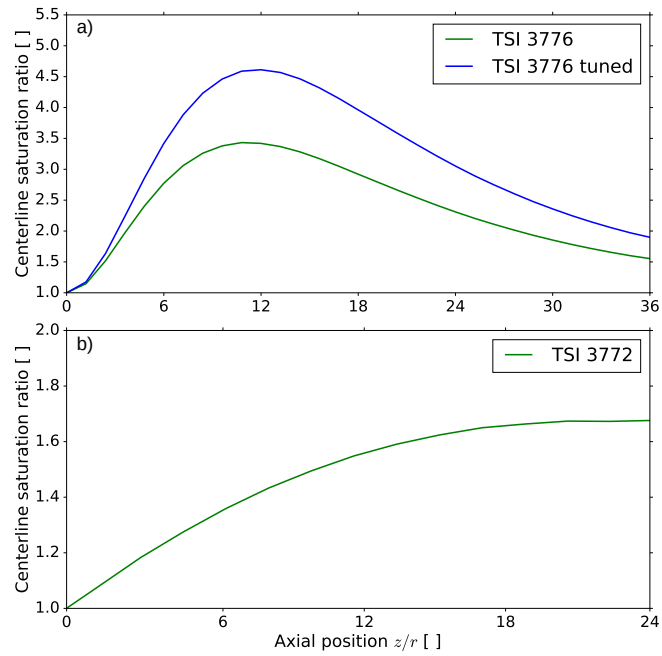


Figure S7. Saturation Ratio in the Condensers: The Figure shows the centerline saturation ratio as a function of the axial distance for the TSI 3776 (Panel a), the tuned TSI 3776 (Panel a) and the TSI 3772 (Panel b).